Kirchhoff prestack depth migration in simple orthorhombic and triclinic models with differently rotated elasticity tensor: comparison with zero-offset travel-time perturbations

Václav Bucha
Department of Geophysics, Faculty of Mathematics and Physics, Charles University in Prague, Ke Karlovu 3, 121 16 Praha 2, Czech Republic,
E-mail: bucha@seis.karlov.mff.cuni.cz

Abstract

We use ray-based Kirchhoff prestack depth migration to calculate migrated sections in simple anisotropic homogeneous velocity models in order to demonstrate the impact of rotation of the tensor of elastic moduli on migrated images. The recorded wave field is generated in velocity models composed of two homogeneous layers separated by a curved interface. The anisotropy of the upper layer is orthorhombic or triclinic with the rotation of the tensor of elastic moduli. We apply the Kirchhoff prestack depth migration to single-layer velocity models with orthorhombic or triclinic anisotropy with a differently rotated tensor of elastic moduli. We show and discuss the errors of the migrated interface caused by incorrect velocity models used for migration. The shifts of zero-offset migrated interface caused by incorrect velocity models are estimated using the linear travel-time perturbations and compared with migrated images. The study is limited to P-waves.

Keywords

3-D Kirchhoff prestack depth migration, anisotropic velocity model, rotation of the tensor of elastic moduli, general elastic anisotropy, orthorhombic anisotropy, triclinic anisotropy, travel-time perturbations

1. Introduction

In this paper we extend results presented by Bucha (2014a, 2014b), where we studied the effect of the rotation of the tensor of elastic moduli (stiffness tensor) on migrated images. The extension includes estimation of shifts of zero-offset migrated interface caused by incorrect velocity models using travel-time perturbations and comparison of them with migrated sections and zero-offset migrated sections.

The dimensions of the velocity model, shot-receiver configuration, methods for calculation of the recorded wave field and the migration are the same as in the previous papers by Bucha (e.g., 2012, 2013, 2014a, 2014b). The reason why we use such simple velocity models is to clearly show the influence of one varying parameter on the migrated image, in this case the influence of rotation angle of a rotated elasticity tensor (stiffness tensor). In more complex velocity model with more realistic parameters, it will be very difficult, maybe impossible, to identify causes of errors in migrated images.

We generate synthetic seismograms using the ray theory which is approximate and we apply ANRAY software package (Gajewski & Pšenčík, 1990). To compute the synthetic recorded wave field, we use simple anisotropic velocity models composed of two homogeneous layers separated by one curved interface that is non-inclined in the direction perpendicular to the source-receiver profiles. The anisotropy in the upper layer is orthorhombic or triclinic with the rotation of the tensor of elastic moduli. Both anisotropies are relatively strong. The angles of rotation are equal to 15, 30 and 45 degrees around axes x_1, x_2 or x_3, respectively. Orthorhombic anisotropy has three mutually perpendicular planes of symmetry. Triclinic anisotropy is not mirror symmetric. It is known that the rotation of elasticity tensor causes the change of velocity in specified direction and consequently affects travel times. The rotation of elasticity tensor also causes asymmetry of the orthorhombic anisotropy. The asymmetry influences differently deflection of two-point rays from the vertical plane containing the source-receiver line (for examples see Bucha 2014a, 2014b).

Then we migrate the synthetic data using 3-D ray-based Kirchhoff prestack depth migration in *correct* and *incorrect* single-layer orthorhombic or triclinic velocity models *with* and *without* the rotation of the elasticity tensor. We utilize MODEL, CRT, FORMS and DATA packages (Červený, Klimeš & Pšenčík, 1988; Bulant, 1996; Bucha & Bulant, 2015). The packages used for calculation of recorded wave field and for migration are independent.

The distribution of elastic moduli in each *correct* velocity model corresponds to the upper layer of the velocity model (*with* the rotation of the elasticity tensor) in which the corresponding synthetic seismograms have been calculated.

Incorrect velocity models have orthorhombic or triclinic anisotropy *without* the rotation of the tensor of elastic moduli. In this way we simulate situations in which we have made an incorrect guess of the anisotropic velocity model for migration.

Migrated sections for *correct* and *incorrect* velocity models were presented already in Bucha (2014a, 2014b). In this paper we estimate shifts of zero-offset migrated interface caused by *incorrect* velocity models using the linear travel-time perturbations (Klimeš, 2002, 2010) and compare them with migrated sections and zero-offset migrated sections calculated in *incorrect* velocity models. For comparison we additionally calculate migrated sections, zero-offset migrated sections and zero-offset travel-time perturbations for the recorded wave field calculated in velocity models with rotated VTI anisotropy in the upper layer. VTI anisotropy is the first element of orthorhombic anisotropy. The angle of rotation is equal to 45 degrees around axes x_1, x_2 or x_3, respectively. We migrate in *incorrect* VTI velocity models *without* the rotation of the tensor of elastic moduli. All calculations are limited to P-waves.

2. Anisotropic velocity models

The dimensions of the velocity models and measurement configurations are derived from the 2-D Marmousi model and dataset (Versteeg & Grau, 1991). The horizontal dimensions of the velocity model are 0 km $\leq x_1 \leq$ 9.2 km, 0 km $\leq x_2 \leq$ 10 km and the depth is 0 km $\leq x_3 \leq$ 3 km.

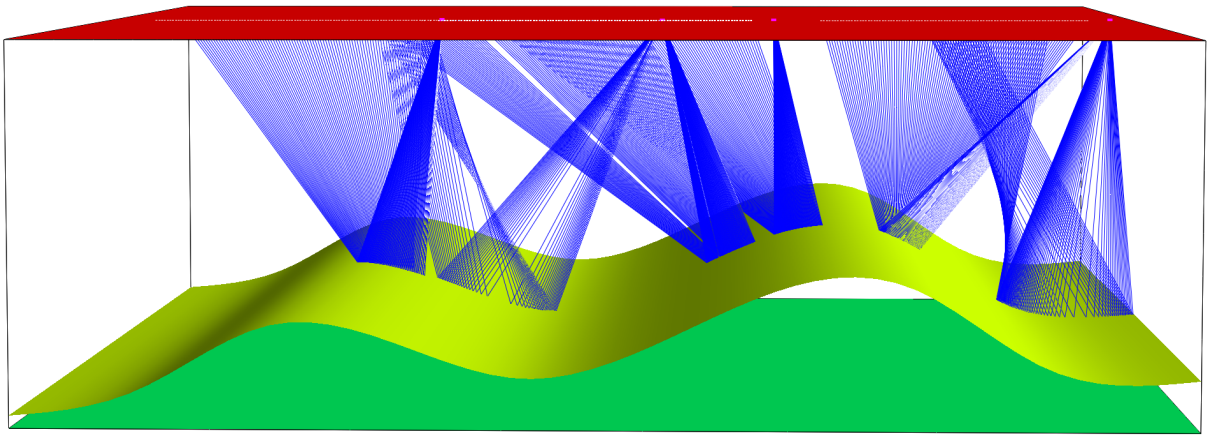

Figure 1. Velocity model with a curved interface. The horizontal dimensions of the velocity model are 0 km $\leq x_1 \leq$ 9.2 km, 0 km $\leq x_2 \leq$ 10 km and the depth is 0 km $\leq x_3 \leq$ 3 km. The velocity model contains one curved interface which is non-inclined in the direction perpendicular to the source-receiver profiles. Two-point rays of the reflected P-wave for one selected profile line (at horizontal coordinate $x_2 = 5$ km) and four shot-receiver configurations (shots 1, 80, 120 and 240 along the profile) are calculated in the velocity model with triclinic anisotropy rotated by 45 degrees around coordinate axis x_2 (TA-X2-45 medium).

2.1 Velocity models for the recorded wave field

The recorded wave field is computed in the velocity models composed of two homogeneous layers separated by one curved interface (see Figure 1). The curved interface is non-inclined in the direction of the x_2 axis which is perpendicular to the source-receiver profiles. The medium in the upper layer of these velocity models is either orthorhombic or triclinic, with the rotation of the elasticity tensor. The bottom layer is isotropic.

Orthorhombic medium without the rotation (OA) is vertically fractured and is composed of two elements (Schoenberg & Helbig, 1997). The first element, a transversely isotropic background medium with a vertical axis of symmetry (VTI), is fairly typical of many shales. The second element is a set of parallel vertical fractures. Orthorhombic anisotropy has three mutually perpendicular planes of symmetry.

The matrix of density-reduced elastic moduli in $\mathrm{km}^2/\mathrm{s}^2$ reads

$$\begin{pmatrix} 9. & 3.6 & 2.25 & 0. & 0. & 0. \\ & 9.84 & 2.4 & 0. & 0. & 0. \\ & & 5.9375 & 0. & 0. & 0. \\ & & & 2. & 0. & 0. \\ & & & & 1.6 & 0. \\ & & & & & 2.182 \end{pmatrix}. \tag{1}$$

Triclinic medium without the rotation (TA) is represented by dry Vosges sandstone (Mensch & Rasolofosaon, 1997). Triclinic anisotropy is asymmetric.

The matrix of density-reduced elastic moduli in $\mathrm{km}^2/\mathrm{s}^2$ reads

$$\begin{pmatrix} 10.3 & 0.9 & 1.3 & 1.4 & 1.1 & 0.8 \\ & 10.6 & 2.1 & 0.2 & -0.2 & -0.6 \\ & & 14.1 & 0. & -0.5 & -1. \\ & & & 5.1 & 0. & 0.2 \\ & & & & 6. & 0. \\ & & & & & 4.9 \end{pmatrix}. \tag{2}$$

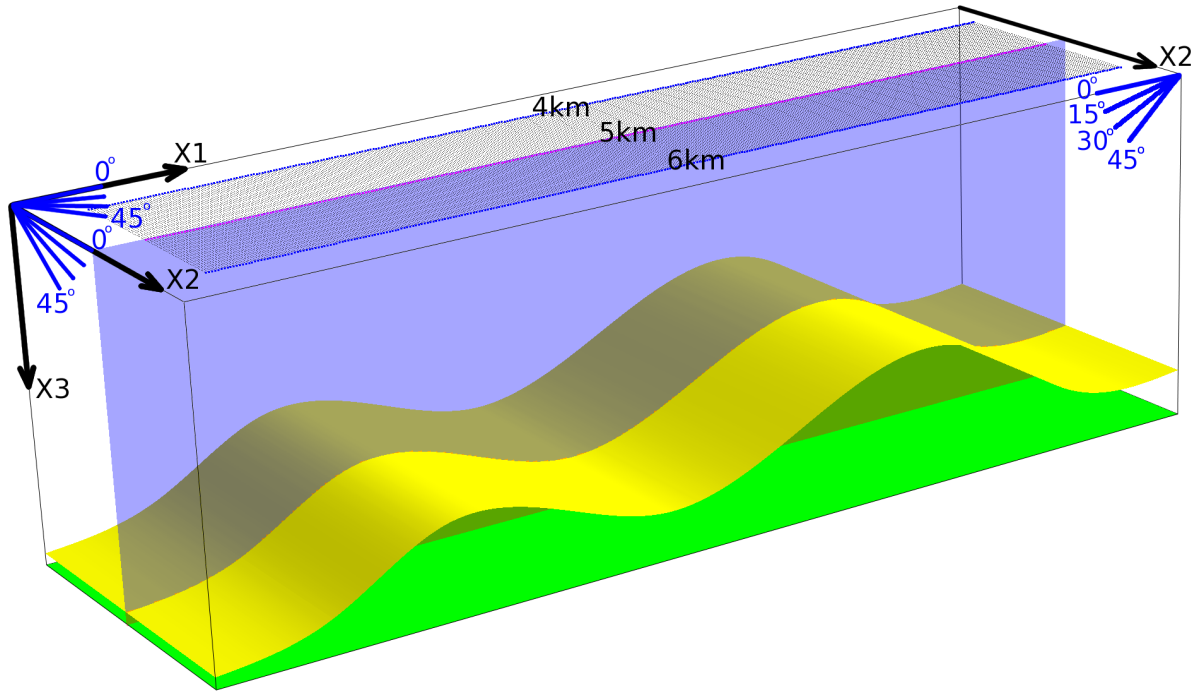

Figure 2. Part of the velocity model with 81 parallel profile lines, the curved interface and the bottom velocity model plane. The horizontal dimensions of the depicted part of the velocity model are 0 km $\leq x_1 \leq$ 9.2 km, 3.5 km $\leq x_2 \leq$ 6.5 km, the depth is 0 km $\leq x_3 \leq$ 3 km. We compute and stack migrated sections in the 2-D plane located in the middle of the shot-receiver configuration, at horizontal coordinate $x_2 = 5$ km. The rotation of the tensor of elastic moduli around axes x_1, x_2 or x_3 is equal to 15, 30 and 45 degrees.

For calculation of the recorded wave field we use nine velocity models with the orthorhombic anisotropy and nine velocity models with the triclinic anisotropy, all with differently rotated tensors of elastic moduli in the upper layer (see Figure 2). The angles of the rotation are 15, 30 and 45 degrees around axes x_1, x_2 or x_3. We utilize specific notation for rotated anisotropies, e.g. OA-X1-15 is for the orthorhombic anisotropy rotated 15 degrees around the axis x_1. The rotation of elasticity tensor causes the change of velocity in specified direction and causes asymmetry of the orthorhombic anisotropy. For rotated matrices of density-reduced elastic moduli in Voigt notation used for calculations see Appendix A. Note that the rotated matrices published in Bucha (2014a, 2014b) were rounded to two decimal places.

The bottom layer in all velocity models is isotropic and the P-wave velocity in the layer is $V_p = 3.6$ km/s. The S-wave velocity is $V_s = V_p/\sqrt{3}$.

2.2 Velocity models for the migration

We migrate in *correct* single-layer velocity models (without the curved interface) with orthorhombic or triclinic anisotropy with the correctly rotated tensors of elastic moduli. The distribution of elastic moduli in *correct* velocity models corresponds to the upper layer of the velocity models (*with* the rotation of the elasticity tensor) in which the synthetic data have been calculated (matrices (4) - (9) in Appendix A).

Additionally we migrate in *incorrect* single-layer velocity models with orthorhombic or triclinic anisotropy *without* the rotation of the tensor of elastic moduli (matrices (1)

and (2)) in order to simulate situations in which we have made an incorrect guess of the anisotropic velocity model for migration.

3. Shots and receivers

The measurement configuration is derived from the Marmousi model and dataset (Versteeg & Grau, 1991). The profile lines are parallel with the x_1 coordinate axis. Each profile line has the following configuration: The first shot is 3 km from the left-hand side of the velocity model, the last shot is 8.975 km from the left-hand side of the velocity model (see Figure 1), the distance between the shots is 0.025 km, and the depth of the shots is 0 km. The total number of shots along one profile line is 240. The number of receivers per shot is 96, the first receiver is located 2.575 km left of the shot location, the last receiver is 0.2 km left of the shot location, the distance between the receivers is 0.025 km, and the depth of the receivers is 0 km. This configuration simulates a simplified towed streamed acquisition geometry.

The 3-D measurement configuration consists of 81 parallel profile lines, see Figure 2. The distance between the parallel profile lines is 0.025 km.

4. Recorded wave field

The recorded wave field in the orthorhombic or triclinic velocity models with the rotation of the tensor of elastic moduli was computed using the ANRAY software package (Gajewski & Pšenčík, 1990). 3-D ray tracing is used to calculate the two-point rays of the reflected P-wave. We then compute the ray-theory seismograms at the receivers.

Orthorhombic anisotropy has three mutually perpendicular planes of symmetry. In the case the shot-receiver configuration is in the plane of symmetry (without rotation of elasticity tensor), the two-point rays stay in the vertical planes corresponding to the individual profiles. The rotation of elasticity tensor causes asymmetry and the two-point rays do not stay in the vertical planes corresponding to the individual profiles even for interfaces non-inclined in the direction perpendicular to the source-receiver profiles. The triclinic asymmetry causes that the two-point rays do not stay in the vertical planes corresponding to the individual profiles. For examples of the deflection of two-point rays from the vertical plane see Bucha (2014a, 2014b). The recorded wave field is equal for all parallel profile lines, because the distribution of elastic moduli in each layer is homogeneous, and the curved interface is independent of the coordinate x_2 perpendicular to the profile lines (2.5-D velocity model, see Figures 1 and 2).

5. Kirchhoff prestack depth migration

We use the MODEL, CRT, FORMS and DATA packages for the 3-D Kirchhoff prestack depth migration (Červený, Klimeš & Pšenčík, 1988; Bulant, 1996; Bucha & Bulant, 2015). The migration consists of two-parametric controlled initial-value ray tracing (Bulant, 1999) from the individual surface points, calculating grid values of travel times and amplitudes by interpolation within ray cells (Bulant & Klimes, 1999), performing the common-shot migration and stacking the migrated images. The shot-receiver configuration consists of 81 parallel profile lines at intervals of 0.025 km (see Figure 2). The first profile line is situated at horizontal coordinate $x_2 = 4$ km and the last profile line is situated at horizontal coordinate $x_2 = 6$ km. For migration we use single-layer velocity models (without the curved interface).

5.1 Migration using the correct velocity models

The distribution of elastic moduli in *correct* single-layer velocity model for migration is the same as the distribution in the upper layer of the velocity model (*with* the rotation of the elasticity tensor) used to calculate the recorded wave field (matrices (4) - (9) in Appendix A).

We perform calculations in *correct* velocity models to demonstrate that the migration algorithm works well. Such migrated sections may be used as a reference for comparison with the migrated sections calculated for *incorrect* velocity models. Migrated sections for *correct* velocity models were presented in papers by Bucha (2014a, 2014b).

5.2 Migration using the incorrect velocity models

In this test, we use the Kirchhoff prestack depth migration to calculate migrated sections in *incorrect* homogeneous velocity models. We simulate situations in which we have made an incorrect guess of the rotation of the tensor of elastic moduli around axes x_1, x_2 or x_3. So we migrate in *incorrect* single-layer velocity models with orthorhombic (OA medium) or triclinic (TA medium) anisotropy *without* the rotation of the tensor of elastic moduli defined by matrices (1) or (2).

Migrated sections for *incorrect* velocity models were presented already in Bucha (2014a, 2014b). To compare and evaluate results of imaging we additionally calculate zero-offset travel-time perturbations and zero-offset migrated sections.

5.2.1 Zero-offset travel-time perturbations

For calculation of travel-time perturbations we utilize theory derived by Klimeš (2002, 2010). In smooth media, the third-order and higher-order spatial derivatives of travel time and all perturbation derivatives of travel time can be calculated along the rays by simple numerical quadratures using the equations derived by Klimeš (2002). Lately, Klimeš (2010) derives the explicit equations for transforming any spatial and perturbation derivatives of travel time at a general smooth curved interface between two arbitrary media.

In our case we calculate only first-order travel-time perturbations and we use the MODEL, CRT, FORMS and DATA packages. At first we compute rays (zero-offset exploding reflector) from sources situated at curved interface (crosses in Figures 3, 4, 5, 6, 7 and 8) and we are looking for end points at the model surface. Then we perform ray tracing from the points at the model surface and calculate Green function. Results of Green function, travel times and their derivatives, computed sequently for velocity models with and without the rotation of elastic moduli, are the base for calculation of travel-time perturbations and transformation to spatial coordinates (centred octagons in Figures 3, 4, 5, 6, 7 and 8).

5.2.2 Zero-offset migration

For zero-offset migration we use the same 3-D Kirchhoff prestack depth migration (packages MODEL, CRT, FORMS and DATA) specified in Section 5. Only the measurement configuration differs, calculations are performed from shots that coincide with receivers.

5.2.3 Orthorhombic anisotropy

Figure 3 shows three stacked migrated sections for the recorded wave field calculated in velocity models with the orthorhombic anisotropy with the rotation of the tensor of elastic moduli around axes x_1, x_2 or x_3 in the upper layer. Model for migration has the orthorhombic anisotropy without the rotation of the elasticity tensor (OA). We display only migrated sections for the angle of rotation 45 degrees. Results for angles of rotation 15 and 30 degrees are analogous and the errors of migrated interface increase with the angle of the rotation (for migrated sections see Bucha, 2014a).

Figure 3a shows the result of the migration for the recorded wave field calculated in velocity model with the rotation around axis x_1 (OA-X1-45). The migrated interface is shifted vertically upwards (undermigrated) and the shift increases with the angle of the rotation. This fact indicates that velocity models with rotated elasticity tensors are faster for reflected P-wave than velocity models without rotation. The two-point rays are considerably deflected from the vertical plane corresponding to the profile line (see Bucha, 2014a). The angle of deflection increases with the angle of the rotation. Zero-offset travel-time perturbations (centred octagons) coincide with migrated interface.

Figure 3b displays migrated section for the recorded wave field calculated in velocity model with the rotation around axis x_2 (OA-X2-45). Note the nearly correctly migrated interface in the horizontal range of approximately $5-6$ km for all angles of the rotation. So the velocity of reflected P-waves for this part of the interface in velocity models with rotated elasticity tensor is nearly the same as the velocity in the model without the rotation. The segments of the interface in horizontal ranges of approximately $2-5$ km and $6-8$ km are defocused and mispositioned (undermigrated), i.e. the velocity of reflected P-waves in models with rotated elasticity tensor is greater than the velocity in the model without the rotation. Surprisingly the two-point rays in this case stay nearly in the vertical plane corresponding to the profile line (see Bucha, 2014a). Zero-offset travel-time perturbations (centred octagons) don't coincide in ranges of approximately $3-5$ km and $6-8$ km with migrated interface.

Figure 3c shows stacked migrated section for the recorded wave field calculated in velocity model with the rotation around axis x_3 (OA-X3-45). The migrated interface is slightly shifted vertically upwards (undermigrated). The shift increases with the angle of the rotation and is noticeable for the angle 45 degrees. The two-point rays do not stay in the vertical plane corresponding to the profile line. Zero-offset travel-time perturbations (centred octagons) coincide with migrated interface.

Figure 4 displays zero-offset migrated interface and zero-offset travel-time perturbations for the recorded wave field calculated in velocity model with the rotation around axis x_2 (OA-X2-45). We try to explain the reason why travel-time perturbations in ranges of approximately $3-5$ km and $6-8$ km don't coincide with migrated interface (Figure 4a). We suppose that the reason is too big difference between velocity model used for recorded wavefield and velocity model used for migration, in specified direction. Consequently both perturbation and migration methods don't work properly.

To prove this hypothesis we calculate zero-offset travel-time perturbations and zero-offset migrations for velocity models with decreased difference between models used for recorded wave field and migration. We look for velocity models for which the coincidence

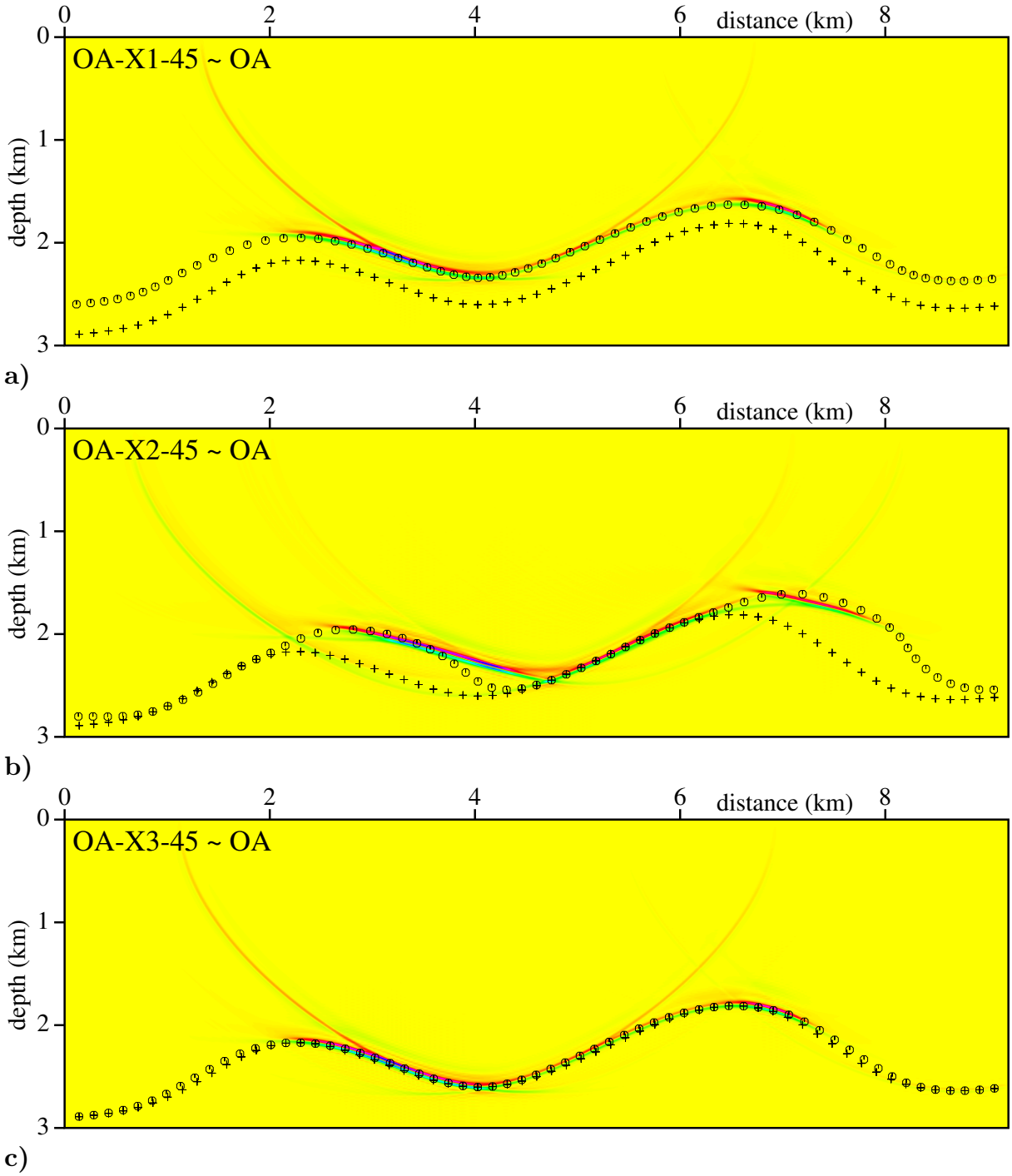

Figure 3. Stacked migrated sections calculated in the incorrect velocity models with orthorhombic anisotropy (OA) without the rotation of the tensor of elastic moduli. The correct anisotropy is orthorhombic with **a)** 45 degree rotation of the tensor of elastic moduli around the x_1 axis (OA-X1-45), **b)** 45 degree rotation of the tensor of elastic moduli around the x_2 axis (OA-X2-45) and **c)** 45 degree rotation of the tensor of elastic moduli around the x_3 axis (OA-X3-45). 81×240 common-shot prestack depth migrated sections, corresponding to 81 profile lines and 240 sources along each profile line, have been stacked. The crosses denote the interface in the velocity models used to compute the recorded wave field. Centred octagons denote zero-offset travel-time perturbations.

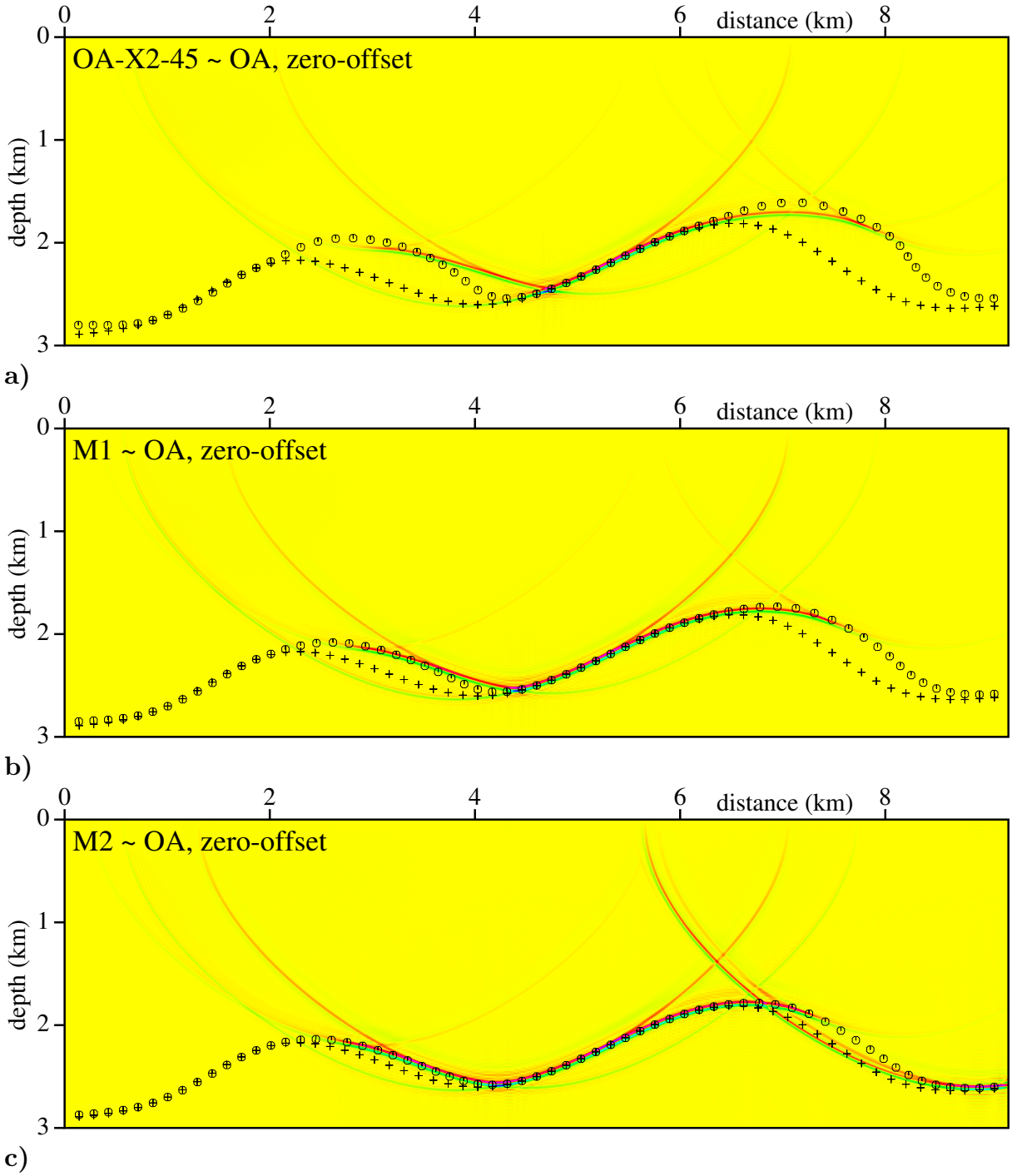

Figure 4. Zero-offset stacked migrated sections calculated in the incorrect velocity models with orthorhombic anisotropy (OA) without the rotation of the tensor of elastic moduli. The correct anisotropy is orthorhombic with **a)** 45 degree rotation of the tensor of elastic moduli around the x_2 axis (OA-X2-45), **b)** arithmetic mean (M1) of elastic moduli and **c)** arithmetic mean (M2) of elastic moduli. The crosses denote the interface in the velocity models used to compute the recorded wave field. Centred octagons denote zero-offset travel-time perturbations.

between perturbations and migrated interface is acceptable. In the first iteration we simply determine mean values (M1) of rotated elastic moduli (OA-X2-45) and elastic moduli (OA) without rotation.

$$(\text{M1}) = \frac{(\text{OA-X2-45}) + (\text{OA})}{2}$$

Then we calculate recorded wave field in velocity model (M1) and migrate in velocity model (OA). We check the difference between zero-offset travel-time perturbations and zero-offset migrations. Figure 4b displays the difference that is smaller but still too big. We continue with the second iteration towards velocity model used for migration and determine mean values (M2) of rotated elastic moduli (M1) and elastic moduli for migration (OA) without rotation.

$$(\text{M2}) = \frac{1}{4}(\text{OA-X2-45}) + \frac{3}{4}(\text{OA})$$

We calculate recorded wave field in velocity model (M2) and migrate in velocity model (OA). The coincidence of zero-offset travel-time perturbations and zero-offset migrations is very good now (see Figure 4c).

5.2.4 VTI background medium

Orthorhombic medium without the rotation (OA) is vertically fractured and is composed of two elements (Schoenberg & Helbig, 1997). The first element is a transversely isotropic background medium with a vertical axis of symmetry (VTI). The second element is a set of parallel vertical fractures. For comparison we additionally calculate migrated sections and zero-offset travel-time perturbations for the recorded wave field calculated in velocity models with the first VTI element in the upper layer. The matrix of density-reduced elastic moduli in km^2/s^2 without the rotation (VTI) reads

$$\begin{pmatrix} 10.0 & 4.0 & 2.5 & 0.0 & 0.0 & 0.0 \\ & 10.0 & 2.5 & 0.0 & 0.0 & 0.0 \\ & & 6.0 & 0.0 & 0.0 & 0.0 \\ & & & 2.0 & 0.0 & 0.0 \\ & & & & 2.0 & 0.0 \\ & & & & & 3.0 \end{pmatrix}. \tag{3}$$

Figure 5 displays migrated interfaces and zero-offset travel-time perturbations for the recorded wave field calculated in velocity models with VTI anisotropy rotated 45 degrees around axes x_1, x_2 and x_3 (for rotated matrices see Appendix A7). Model for migration has the VTI anisotropy without the rotation of the elasticity tensor (matrix (3)). Results of migration are similar to orthorhombic case. We observe slightly greater mispositioning for rotations around axes x_1, x_2 (VTI-X1-45, VTI-X2-45). Result for the rotation around axis x_3 (VTI-X3-45) is due to symmetry the same as without rotation (VTI) and demonstrates that the migration and perturbation algorithms work well in correct velocity model.

Figure 6 displays zero-offset migrated interface and zero-offset travel-time perturbations for the recorded wave field calculated in velocity model with the rotation around axis x_2 (VTI-X2-45). Analogously as for orthorhombic anisotropy we observe that travel-time perturbations in ranges of approximately $3 - 5$ km and $6 - 8$ km do not coincide with migrated interface (Figure 6a). We suppose that the reason is likewise too big difference between velocity model used for recorded wavefield and velocity model used for migration, in specified direction (Figures 6b, 6c).

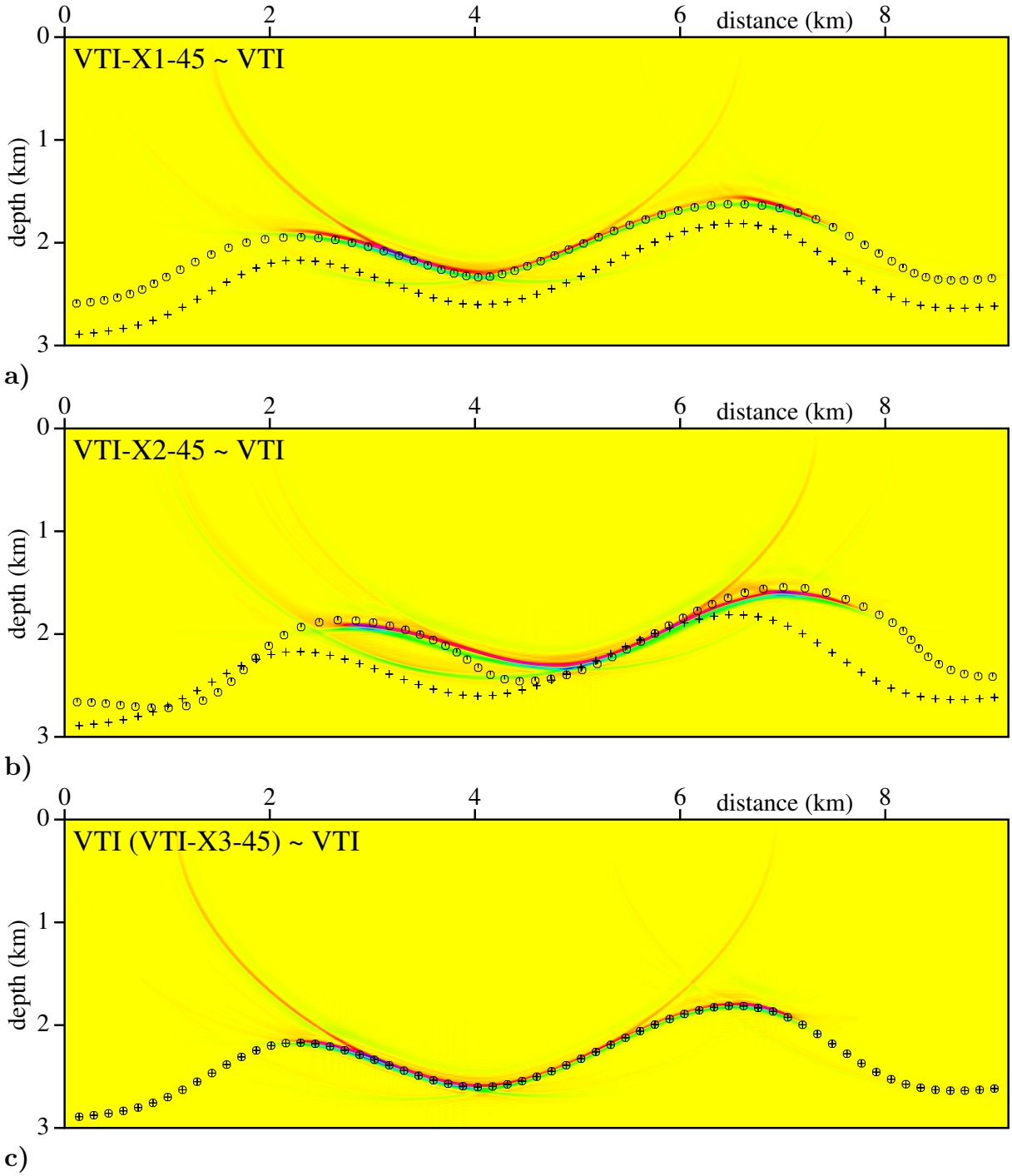

Figure 5. Stacked migrated sections calculated in the incorrect velocity models with transversely isotropic background medium with a vertical axis of symmetry (VTI) without the rotation of the tensor of elastic moduli. The correct anisotropy is transversely isotropic background medium with a vertical axis of symmetry with **a)** 45 degree rotation of the tensor of elastic moduli around the x_1 axis (VTI-X1-45), **b)** 45 degree rotation of the tensor of elastic moduli around the x_2 axis (VTI-X2-45) and **c)** 45 degree rotation of the tensor of elastic moduli around the x_3 axis (VTI-X3-45) that is due to symmetry the same as without rotation (VTI). 81×240 common-shot prestack depth migrated sections, corresponding to 81 profile lines and 240 sources along each profile line, have been stacked. The crosses denote the interface in the velocity models used to compute the recorded wave field. Centred octagons denote zero-offset travel-time perturbations.

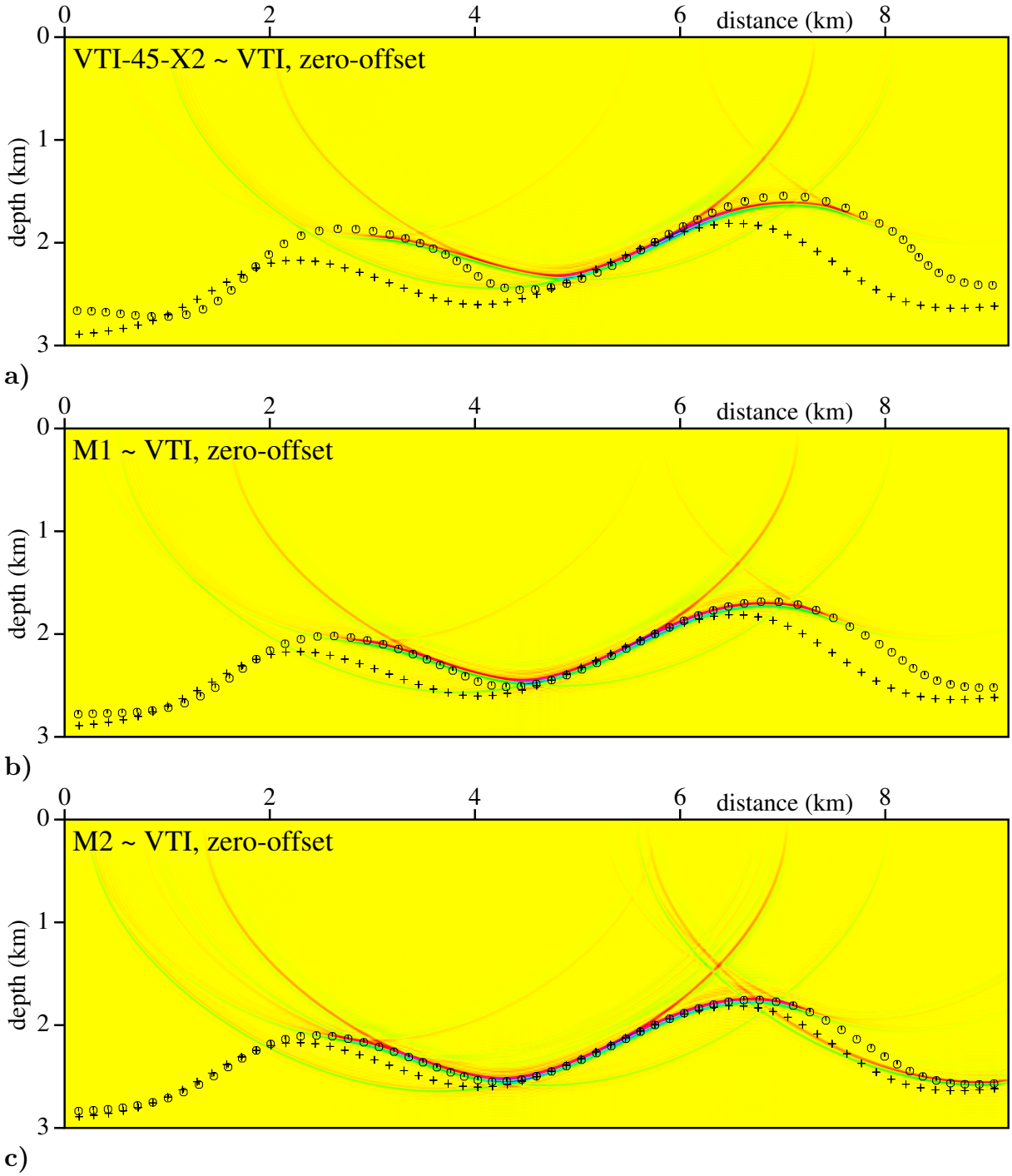

Figure 6. Zero-offset stacked migrated sections calculated in the incorrect velocity models with transversely isotropic background medium with a vertical axis of symmetry (VTI) without the rotation of the tensor of elastic moduli. The correct anisotropy is transversely isotropic background medium with a vertical axis of symmetry with **a)** 45 degree rotation of the tensor of elastic moduli around the x_2 axis (VTI-X2-45), **b)** arithmetic mean (M1) of elastic moduli and **c)** arithmetic mean (M2) of elastic moduli. The crosses denote the interface in the velocity models used to compute the recorded wave field. Centred octagons denote zero-offset travel-time perturbations.

5.2.5 Triclinic anisotropy

Figure 7 shows three stacked migrated sections for the recorded wave field calculated in velocity models with the triclinic anisotropy with the rotation of the tensor of elastic moduli around axes x_1, x_2 or x_3 in the upper layer. Model for migration has the triclinic anisotropy without the rotation of the elasticity tensor (TA). We display only migrated sections for the angle of rotation 45 degrees. Results for angles of rotation 15 and 30 degrees are analogous and the errors of migrated interface increase with the angle of the rotation (for migrated sections see Bucha, 2014b).

Figure 7a shows the result of the migration for the recorded wave field calculated in velocity model with the rotation around axis x_1 (TA-X1-45). The migrated interface is slightly shifted vertically downwards (overmigrated) and the shift increases with the angle of the rotation. This fact indicates that velocity models with rotated elasticity tensors are slower for reflected P-wave than models without rotation. The two-point rays are deflected from the vertical plane corresponding to the profile line (see Bucha, 2014b). The angle of deflection increases with the angle of the rotation. Zero-offset travel-time perturbations (centred octagons) coincide with migrated interface.

Figure 7b displays migrated section for the recorded wave field calculated in velocity model with the rotation around axis x_2 (TA-X2-45). Note the nearly correctly migrated interface in the horizontal range of approximately $4-6$ km for all angles of the rotation. So the velocity of reflected P-waves for this part of the interface in velocity models with rotated elasticity tensor is nearly the same as the velocity in velocity model without the rotation. The segments of the interface in horizontal ranges of approximately $2-4$ km and $6-8$ km are defocused and mispositioned (overmigrated), i.e. the velocity of reflected P-waves in velocity models with rotated elasticity tensor is lower than the velocity in the model without the rotation. The two-point rays do not stay in the vertical plane corresponding to the profile line. Zero-offset travel-time perturbations (centred octagons) don't coincide in ranges of approximately $2-4$ km and $6-8$ km with migrated interface.

Figure 7c shows stacked migrated section for the recorded wave field calculated in velocity model with the rotation around axis x_3 (TA-X3-45). The segments of the interface in horizontal ranges of approximately $2-4$ km and $6-8$ km are slightly defocused and mispositioned (undermigrated), while the interface in the horizontal range of approximately $4-6$ km is nearly correctly migrated. The two-point rays do not stay in the vertical plane corresponding to the profile line. The deflection of rays from the vertical plane is smaller than deflections of rays for rotations around axes x_1 or x_2 (see Bucha, 2014b). Zero-offset travel-time perturbations (centred octagons) coincide acceptably with migrated interface.

Figure 8 displays zero-offset migrated interface and zero-offset travel-time perturbations for the recorded wave field calculated in the model with the rotation around axis x_2 (TA-X2-45). Analogously as for orthorhombic anisotropy we try to explain the reason why travel-time perturbations in ranges of approximately $2-4$ km and $6-8$ km don't coincide with migrated interface (Figure 8a). We again suppose that the reason is too big difference between the model used for recorded wavefield and the model used for migration, in specified direction. Consequently both perturbation and migration methods don't work properly.

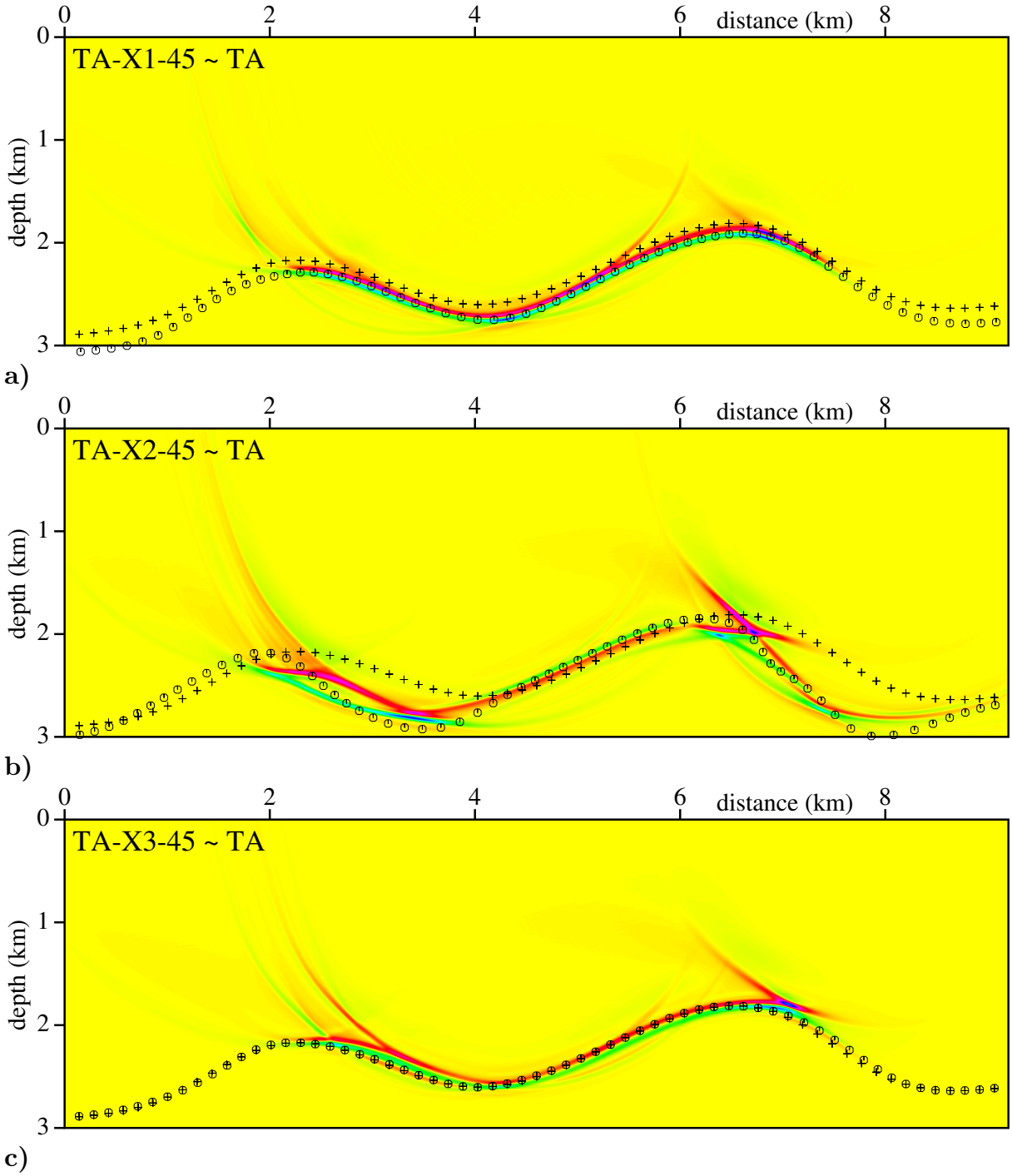

Figure 7. Stacked migrated sections calculated in the incorrect velocity models with triclinic anisotropy (TA) without the rotation of the tensor of elastic moduli. The correct anisotropy is triclinic with **a)** 45 degree rotation of the tensor of elastic moduli around the x_1 axis (TA-X1-45), **b)** 45 degree rotation of the tensor of elastic moduli around the x_2 axis (TA-X2-45) and **c)** 45 degree rotation of the tensor of elastic moduli around the x_3 axis (TA-X3-45). 81×240 common-shot prestack depth migrated sections, corresponding to 81 profile lines and 240 sources along each profile line, have been stacked. The crosses denote the interface in the velocity models used to compute the recorded wave field. Centred octagons denote zero-offset travel-time perturbations.

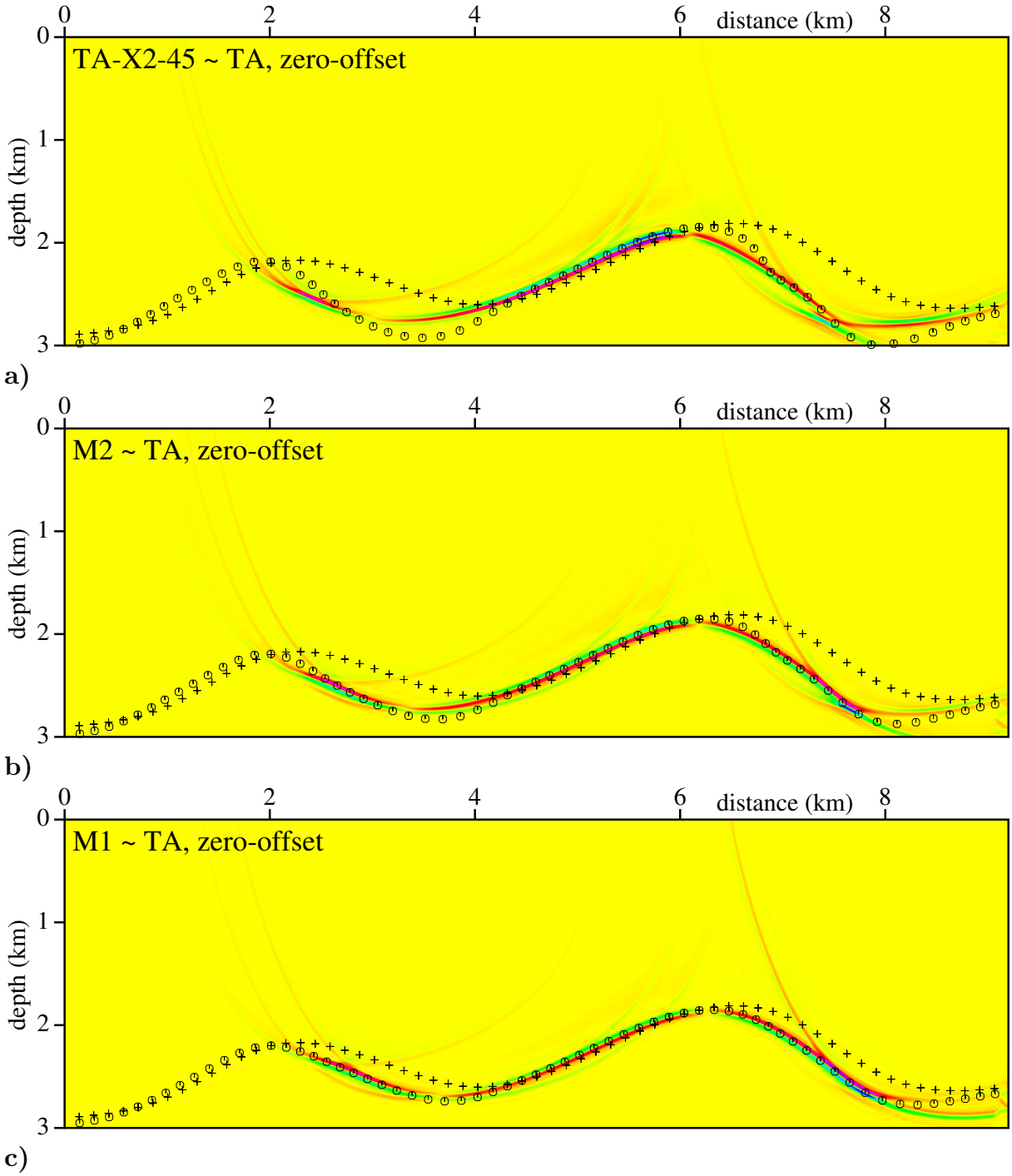

Figure 8. Zero-offset stacked migrated sections calculated in the incorrect velocity models with triclinic anisotropy (TA) without the rotation of the tensor of elastic moduli. The correct anisotropy is triclinic with **a)** 45 degree rotation of the tensor of elastic moduli around the x_2 axis (TA-X2-45), **b)** arithmetic mean (M2) of elastic moduli and **c)** arithmetic mean (M1) of elastic moduli. The crosses denote the interface in the velocity models used to compute the recorded wave field. Centred octagons denote zero-offset travel-time perturbations.

To prove this hypothesis we calculate zero-offset travel-time perturbations and zero-offset migrations for velocity models with decreased difference between velocity models used for recorded wave field and migration. We look for velocity models for which the coincidence between perturbations and migrated interface is acceptable. In the first iteration we simply determine mean values (M1) of rotated elastic moduli (TA-X2-45) and elastic moduli (TA) without rotation.

$$(\text{M1}) = \frac{(\text{TA-X2-45}) + (\text{TA})}{2}$$

Now we calculate recorded wave field in velocity model (M1) and migrate in velocity model (TA). We check the difference between zero-offset travel-time perturbations and zero-offset migrations. Figure 8c displays the difference that is very small and acceptable. We continue with the second iteration towards velocity model used for recorded wave field and determine mean values (M2) of rotated elastic moduli (M1) and rotated elastic moduli (TA-X2-45).

$$(\text{M2}) = \frac{3}{4}(\text{TA-X2-45}) + \frac{1}{4}(\text{TA})$$

We calculate recorded wave field in velocity model (M2) and migrate in velocity model (TA). Figure 8b shows that the coincidence of zero-offset travel-time perturbations and zero-offset migrations is better than Figure 8a but not good.

6. Conclusions

In order to study the impact of rotation of the tensor of elastic moduli on migrated images, we generated synthetic seismograms using the ray theory in simple homogeneous two-layer velocity models with orthorhombic, VTI or triclinic anisotropy with differently rotated tensors of elastic moduli (stiffness tensors). VTI anisotropy is the first element of orthorhombic anisotropy. Anisotropies are relatively strong. Then we applied 3-D ray-based Kirchhoff prestack depth migration to *correct* and *incorrect* homogeneous single-layer velocity models with orthorhombic, VTI or triclinic anisotropy. *Correct* velocity models have anisotropy *with* the correct rotation of the elasticity tensor. *Incorrect* velocity models have anisotropy *without* the rotation and in this way we simulate situations in which we have made an incorrect guess of the rotation of the tensor of elastic moduli. To check the results we calculated zero-offset travel-time perturbations and zero-offset migration. The study has been limited to P-waves.

Calculation of synthetic seismograms showed for some rotations of the elasticity tensor considerable deflection of two-point rays from the vertical plane caused by anisotropic asymmetry (see Bucha, 2014a, 2014b). We observed the greatest deviation of two-point rays from vertical plane for rotation around coordinate axis x_1 (horizontal axis parallel with profile lines).

For migration in *correct* velocity model with orthorhombic anisotropy *with* the rotation of the tensor of elastic moduli around x_1, x_2 or x_3 axes, the migrated interface in the final stacked image coincides nearly perfectly with the interface in velocity model used to compute the recorded wave field (see Bucha, 2014a).

In the case of *correct* velocity model with triclinic anisotropy *with* the rotation of the tensor of elastic moduli around axes x_1 and x_3, the migrated interface in the final stacked image coincides nearly perfectly with the interface in velocity model used to compute the recorded wave field. For rotation around the axis x_2 we observed nearly vanishing part of the migrated interface caused by zero reflection coefficient and phase

change decreasing amplitudes of synthetic seismograms, and by worse illumination of the interface by rays (see Bucha, 2014b). In our previous study of sensitivity of migration to inaccurate anisotropy we observed nearly the same vanishing part of the migrated interface caused by different phenomenon, the erroneous rotation of single common-shot images (Bucha, 2012).

Migration in *incorrect* velocity models with orthorhombic, VTI or triclinic anisotropy *without* the rotation of the elasticity tensor showed mispositioning, distortion and defocusing of the migrated interface. The shape of errors of the migrated interface depend on the axis around which we rotate, on rotation angle and on the dip of the interface. We observed the smallest errors for rotations around the axis x_3 (vertical) and the greatest distortions for rotations around the axis x_2 (horizontal axis perpendicular to the source-receiver profiles). The errors of the migrated interface increase with the angle of the rotation for all rotation axes.

Estimation of the shifts of zero-offset migrated interface caused by incorrect velocity models using the linear travel-time perturbations is very fast. Results of this method were in our tests very good with one exception: comparison of zero-offset travel-time perturbations and migrated interfaces showed other discrepancies for rotations around horizontal axis perpendicular to the source-receiver profiles (axis x_2) for all three anisotropies. While for rotations around axes x_1 and x_3 migrated interface coincides with travel-time perturbations very well, for rotations around the axis x_2 we observed in some ranges big differences between migrated interface and travel-time perturbations.

In our simple synthetic tests, the errors in images caused by rotated elasticity tensor are in some directions considerable. Moreover, we observed for specific rotation and direction big distortions of the image where perturbation and migration methods don't work properly. The use of perturbation method helped us to reveal and explain this type of distortions caused by too big differences between velocity models for synthetic data and migration in specific direction. We assume that interaction with other errors caused by incorrect anisotropy, incorrect heterogeneities, incorrect dip and inclination of the interfaces, etc., makes it very difficult to identify specific errors in the images of a real structure.

Appendix A: Rotated matrices

Appendix A1: Orthorhombic anisotropy with the rotation around axis X1

The matrix of density-reduced elastic moduli A_{ij} in $\mathrm{km}^2/\mathrm{s}^2$ for the rotation angle around axis x_1 equal to

a) 15 degrees (OA-X1-15) reads

$$\begin{pmatrix} 9.00000 & 3.50957 & 2.34043 & 0.33750 & 0.00000 & 0.000000 \\ & 9.39249 & 2.58609 & 0.81014 & 0.00000 & 0.000000 \\ & & 6.01282 & 0.16549 & 0.00000 & 0.000000 \\ & & & 2.18609 & 0.00000 & 0.000000 \\ & & & & 1.63899 & 0.145505 \\ & & & & & 2.143014 \end{pmatrix}, \tag{4a}$$

b) 30 degrees (OA-X1-30) reads

$$\begin{pmatrix} 9.00000 & 3.26250 & 2.58750 & 0.58457 & 0.00000 & 0.00000 \\ & 8.30609 & 2.95828 & 1.16724 & 0.00000 & 0.00000 \\ & & 6.35484 & 0.52259 & 0.00000 & 0.00000 \\ & & & 2.55828 & 0.00000 & 0.00000 \\ & & & & 1.74550 & 0.25201 \\ & & & & & 2.03650 \end{pmatrix}, \tag{4b}$$

c) 45 degrees (OA-X1-45) reads

$$\begin{pmatrix} 9.00000 & 2.92500 & 2.92500 & 0.67500 & 0.00000 & 0.00000 \\ & 7.14437 & 3.14437 & 0.97562 & 0.00000 & 0.00000 \\ & & 7.14437 & 0.97562 & 0.00000 & 0.00000 \\ & & & 2.74437 & 0.00000 & 0.00000 \\ & & & & 1.89100 & 0.29100 \\ & & & & & 1.89100 \end{pmatrix}. \tag{4c}$$

Appendix A2: Orthorhombic anisotropy with the rotation around axis X2

The matrix of density-reduced elastic moduli A_{ij} in $\mathrm{km}^2/\mathrm{s}^2$ for the rotation angle around axis x_2 equal to

a) 15 degrees (OA-X2-15) reads

$$\begin{pmatrix} 8.54251 & 3.51961 & 2.50234 & 0.00000 & -0.81988 & 0.00000 \\ & 9.84000 & 2.48038 & 0.00000 & -0.30000 & 0.00000 \\ & & 5.89030 & 0.00000 & 0.05426 & 0.00000 \\ & & & 2.01219 & 0.00000 & -0.04550 \\ & & & & 1.85234 & 0.00000 \\ & & & & & 2.16981 \end{pmatrix}, \tag{5a}$$

b) 30 degrees (OA-X2-30) reads

$$\begin{pmatrix} 7.47730 & 3.30000 & 3.00700 & 0.00000 & -1.10010 & 0.00000 \\ & 9.84000 & 2.70000 & 0.00000 & -0.51960 & 0.00000 \\ & & 5.94610 & 0.00000 & -0.22600 & 0.00000 \\ & & & 2.04550 & 0.00000 & -0.07880 \\ & & & & 2.35700 & 0.00000 \\ & & & & & 2.13650 \end{pmatrix}, \tag{5b}$$

c) 45 degrees (OA-X2-45) reads

$$\begin{pmatrix} 6.45937 & 3.00000 & 3.25937 & 0.00000 & -0.76562 & 0.00000 \\ & 9.84000 & 3.00000 & 0.00000 & -0.60000 & 0.00000 \\ & & 6.45937 & 0.00000 & -0.76562 & 0.00000 \\ & & & 2.09100 & 0.00000 & -0.09100 \\ & & & & 2.60937 & 0.00000 \\ & & & & & 2.09100 \end{pmatrix}. \tag{5c}$$

Appendix A3: Orthorhombic anisotropy with the rotation around axis X3

The matrix of density-reduced elastic moduli A_{ij} in km^2/s^2 for the rotation angle around axis x_3 equal to

a) 15 degrees (OA-X3-15) reads

$$\begin{pmatrix} 8.87427 & 3.78200 & 2.26005 & 0.00000 & 0.00000 & 0.21023 \\ & 9.60173 & 2.38995 & 0.00000 & 0.00000 & -0.42023 \\ & & 5.93750 & 0.00000 & 0.00000 & -0.03750 \\ & & & 1.97321 & -0.10000 & 0.00000 \\ & & & & 1.62679 & 0.00000 \\ & & & & & 2.36400 \end{pmatrix}, \tag{6a}$$

b) 30 degrees (OA-X3-30) reads

$$\begin{pmatrix} 8.66400 & 4.14600 & 2.28750 & 0.00000 & 0.00000 & 0.13337 \\ & 9.08400 & 2.36250 & 0.00000 & 0.00000 & -0.49710 \\ & & 5.93750 & 0.00000 & 0.00000 & -0.06495 \\ & & & 1.90000 & -0.17321 & 0.00000 \\ & & & & 1.70000 & 0.00000 \\ & & & & & 2.72800 \end{pmatrix}, \tag{6b}$$

c) 45 degrees (OA-X3-45) reads

$$\begin{pmatrix} 8.69200 & 4.32800 & 2.32500 & 0.00000 & 0.00000 & -0.21000 \\ & 8.69200 & 2.32500 & 0.00000 & 0.00000 & -0.21000 \\ & & 5.93750 & 0.00000 & 0.00000 & -0.07500 \\ & & & 1.80000 & -0.20000 & 0.00000 \\ & & & & 1.80000 & 0.00000 \\ & & & & & 2.91000 \end{pmatrix}. \tag{6c}$$

Appendix A4: Triclinic anisotropy with the rotation around axis X1

The matrix of density-reduced elastic moduli A_{ij} in km^2/s^2 for the rotation angle around axis x_1 equal to

a) 15 degrees (TA-X1-15) reads

$$\begin{pmatrix} 10.3000 & 0.2268 & 1.9732 & 1.1124 & 1.2696 & 0.4880 \\ & 10.6416 & 2.1929 & -0.2901 & -0.4007 & -0.6451 \\ & & 13.8727 & -0.4117 & -0.6896 & -0.7192 \\ & & & 5.1929 & 0.1432 & 0.2445 \\ & & & & 5.9263 & -0.2750 \\ & & & & & 4.9737 \end{pmatrix}, \tag{7a}$$

b) 30 degrees (TA-X1-30) reads

$$\begin{pmatrix} 10.3000 & -0.2124 & 2.4124 & 0.5268 & 1.3526 & 0.1428 \\ & 11.1964 & 2.2054 & -0.7469 & -0.6748 & -0.6187 \\ & & 13.2929 & -0.6686 & -0.7315 & -0.4169 \\ & & & 5.2054 & 0.2491 & 0.1717 \\ & & & & 5.7250 & -0.4763 \\ & & & & & 5.1750 \end{pmatrix}, \tag{7b}$$

c) 45 degrees (TA-X1-45) reads

$$\begin{pmatrix} 10.3000 & -0.3000 & 2.5000 & -0.2000 & 1.3435 & -0.2121 \\ & 12.1250 & 2.1250 & -0.9750 & -0.9546 & -0.4596 \\ & & 12.5250 & -0.7750 & -0.6718 & -0.1768 \\ & & & 5.1250 & 0.2475 & 0.0354 \\ & & & & 5.4500 & -0.5500 \\ & & & & & 5.4500 \end{pmatrix}. \tag{7c}$$

Appendix A5: Triclinic anisotropy with the rotation around axis X2

The matrix of density-reduced elastic moduli A_{ij} in $\mathrm{km}^2/\mathrm{s}^2$ for the rotation angle around axis x_2 equal to

a) 15 degrees (TA-X2-15) reads

$$\begin{pmatrix} 11.6849 & 0.8804 & 0.4697 & 1.0859 & 1.3730 & 0.9943 \\ & 10.6000 & 2.1196 & 0.3485 & 0.1268 & -0.5278 \\ & & 14.3758 & 0.3182 & 0.0967 & -0.8252 \\ & & & 4.9866 & -0.2216 & 0.2232 \\ & & & & 5.1697 & -0.5253 \\ & & & & & 5.0134 \end{pmatrix}, \tag{8a}$$

b) 30 degrees (TA-X2-30) reads

$$\begin{pmatrix} 12.8749 & 1.0268 & 0.1947 & 0.7343 & 0.8109 & 0.8281 \\ & 10.6000 & 1.9732 & 0.4732 & 0.4196 & -0.4196 \\ & & 13.7357 & 0.5781 & 1.1346 & -0.3013 \\ & & & 4.8768 & -0.1353 & 0.1866 \\ & & & & 4.8947 & -0.9781 \\ & & & & & 5.1232 \end{pmatrix}, \tag{8b}$$

c) 45 degrees (TA-X2-45) reads

$$\begin{pmatrix} 13.3500 & 1.3000 & 0.7500 & 0.5657 & 0.1500 & 0.4243 \\ & 10.6000 & 1.7000 & 0.5657 & 0.6000 & -0.2828 \\ & & 12.1500 & 0.5657 & 1.7500 & 0.4243 \\ & & & 4.8000 & 0.1414 & 0.1000 \\ & & & & 5.4500 & -1.1314 \\ & & & & & 5.2000 \end{pmatrix}. \tag{8c}$$

Appendix A6: Triclinic anisotropy with the rotation around axis X3

The matrix of density-reduced elastic moduli A_{ij} in $\mathrm{km}^2/\mathrm{s}^2$ for the rotation angle around axis x_3 equal to

a) 15 degrees (TA-X3-15) reads

$$\begin{pmatrix} 9.6451 & 1.4750 & 1.8536 & 1.4402 & 0.6627 & 0.3450 \\ & 10.1049 & 1.5464 & 0.3382 & -0.2075 & -0.2468 \\ & & 14.1000 & -0.1294 & -0.4830 & -1.0660 \\ & & & 5.1603 & 0.2250 & 0.5412 \\ & & & & 5.9397 & 0.1915 \\ & & & & & 5.4750 \end{pmatrix}, \tag{9a}$$

b) 30 degrees (TA-X3-30) reads

$$\begin{pmatrix} 9.6893 & 1.4125 & 2.3660 & 1.1901 & 0.2078 & -0.4191 \\ & 10.1857 & 1.0340 & 0.6455 & -0.2283 & 0.3892 \\ & & 14.1000 & -0.2500 & -0.4330 & -0.8464 \\ & & & 5.3250 & 0.3897 & 0.8181 \\ & & & & 5.7750 & 0.1777 \\ & & & & & 5.4125 \end{pmatrix}, \tag{9b}$$

c) 45 degrees (TA-X3-45) reads

$$\begin{pmatrix} 10.3750 & 0.7750 & 2.7000 & 0.7425 & -0.1061 & -0.7750 \\ & 10.7750 & 0.7000 & 1.0253 & -0.3889 & 0.6250 \\ & & 14.1000 & -0.3536 & -0.3536 & -0.4000 \\ & & & 5.5500 & 0.4500 & 0.8839 \\ & & & & 5.5500 & 0.0354 \\ & & & & & 4.7750 \end{pmatrix}. \tag{9c}$$

Appendix A7: VTI anisotropy with the rotation around axis X1, X2 and X3

The matrix of density-reduced elastic moduli A_{ij} in km^2/s^2 for the rotation angle 45 degrees around axis x_1 (VTI-X1-45) reads

$$\begin{pmatrix} 10.000 & 3.250 & 3.250 & 0.750 & 0.000 & 0.000 \\ & 7.250 & 3.250 & 1.000 & 0.000 & 0.000 \\ & & 7.250 & 1.000 & 0.000 & 0.000 \\ & & & 2.750 & 0.000 & 0.000 \\ & & & & 2.500 & 0.500 \\ & & & & & 2.500 \end{pmatrix}. \tag{10a}$$

The matrix of density-reduced elastic moduli A_{ij} in km^2/s^2 for the rotation angle 45 degrees around axis x_2 (VTI-X2-45) reads

$$\begin{pmatrix} 7.250 & 3.250 & 3.250 & 0.000 & -1.000 & 0.000 \\ & 10.000 & 3.250 & 0.000 & -0.750 & 0.000 \\ & & 7.250 & 0.000 & -1.000 & 0.000 \\ & & & 2.500 & 0.000 & -0.500 \\ & & & & 2.750 & 0.000 \\ & & & & & 2.500 \end{pmatrix}. \tag{10b}$$

The matrix of density-reduced elastic moduli A_{ij} in km^2/s^2 for the rotation angle 45 degrees around axis x_3 (VTI-X3-45) is due to symmetry the same as unrotated matrix (3).

Acknowledgments

The author thanks Luděk Klimeš and Ivan Pšenčík for their help throughout the work on this paper.

The research has been supported by the Grant Agency of the Czech Republic under Contract 16-05237S, by the Ministry of Education of the Czech Republic within Research Project CzechGeo/EPOS LM2015079, and by the members of the consortium "Seismic Waves in Complex 3-D Structures" (see "http://sw3d.cz").

References

Bucha, V. (2012): Kirchhoff prestack depth migration in 3-D simple models: comparison of triclinic anisotropy with simpler anisotropies. *Stud. geophys. geod.*, **56**, 533–552.

Bucha, V. (2013): Kirchhoff prestack depth migration in velocity models with and without vertical gradients: Comparison of triclinic anisotropy with simpler anisotropies. *Seismic Waves in Complex 3-D Structures*, **23**, 45–59, online at "http://sw3d.cz".

Bucha, V. (2014a): Kirchhoff prestack depth migration in orthorhombic velocity models with differently rotated tensors of elastic moduli. *Seismic Waves in Complex 3-D Structures*, **24**, 59–75, online at "http://sw3d.cz".

Bucha, V. (2014b): Kirchhoff prestack depth migration in triclinic velocity models with differently rotated tensors of elastic moduli. *Seismic Waves in Complex 3-D Structures*, **24**, 77–93, online at "http://sw3d.cz".

Bucha, V. & Bulant, P. (eds.) (2015): SW3D-CD-19 (DVD-ROM). *Seismic Waves in Complex 3-D Structures*, **25**, 209-210, online at "http://sw3d.cz".

Bulant, P. (1996): Two-point ray tracing in 3-D. *Pure appl. Geophys.*, **148**, 421–447.

Bulant, P. (1999): Two-point ray-tracing and controlled initial-value ray-tracing in 3-D heterogeneous block structures. *J. seism. Explor.*, **8**, 57–75.

Bulant, P. & Klimes, L. (1999): Interpolation of ray-theory travel times within ray cells. *Geophys. J. int.*, **139**, 273–282.

Červený, V., Klimeš, L. & Pšenčík, I. (1988): Complete seismic-ray tracing in three-dimensional structures. In: Doornbos, D.J. (ed.), *Seismological Algorithms*, Academic Press, New York, pp. 89–168.

Gajewski, D. & Pšenčík, I. (1990): Vertical seismic profile synthetics by dynamic ray tracing in laterally varying layered anisotropic structures. *J. geophys. Res.*, **95B**, 11301–11315.

Klimeš, L. (2002): Second-order and higher-order perturbations of travel time in isotropic and anisotropic media. *Stud. geophys. geod.*, **46**, 213–248.

Klimeš, L. (2010): Transformation of spatial and perturbation derivatives of travel time at a general interface between two general media. *Seismic Waves in Complex 3-D Structures*, **20**, 103–114, online at "http://sw3d.cz".

Mensch, T. & Rasolofosaon, P. (1997): Elastic-wave velocities in anisotropic media of arbitrary symmetry-generalization of Thomsen's parameters ϵ, δ and γ. *Geophys. J. Int.*, **128**, 43–64.

Schoenberg, M. & Helbig, K. (1997): Orthorhombic media: Modeling elastic wave behavior in a vertically fractured earth. *Geophysics*, **62**, 1954–1974.

Versteeg, R. J. & Grau, G. (eds.) (1991): The Marmousi experience. *Proc. EAGE workshop on Practical Aspects of Seismic Data Inversion (Copenhagen, 1990)*, Eur. Assoc. Explor. Geophysicists, Zeist.